# Two-Component Multireference Restricted Active Space Configuration Interaction for the Computation of L-edge X-ray Absorption Spectra

Andrew J. Jenkins,[†,‡] Hang Hu,[¶,‡] Lixin Lu,[†] Michael J. Frisch,[§] and Xiaosong Li[*,†]

†*Department of Chemistry, University of Washington, Seattle, Washington 98195*

‡*Authors contributed equally to this work*

¶*Molecular Engineering and Sciences Institute, University of Washington, Seattle, Washington 98195*

§*Gaussian Inc., 340 Quinnipiac Street, Building 40, Wallingford, Connecticut, 06492*

E-mail: xsli@uw.edu

**Abstract**

X-ray absorption spectroscopy is a powerful probe of local electronic and nuclear structure, providing insights into chemical processes. The theoretical prediction and interpretation of metal L-edge X-ray absorption spectra is complicated by both relativistic effects, including spin-orbit coupling, and by the multiconfigurational nature of the states involved. This work details an exact two-component multireference restricted active space configuration interaction (X2C-MRRASCI) scheme that uses an exact two-component state average complete active space self-consistent-field method (X2C-SA-CASSCF), which includes the spin-orbit coupling in a variational manner, for the accurate description of the electronic structure before using a restricted active

space configuration interaction method to describe the core excited states of the X-ray spectrum. Benchmark calculations are presented for a series of iron containing complexes, with results showing key features of the spectrum being reproduced, including ligand to metal charge transfer and shake-up excitations.

# 1 Introduction

X-ray absorption spectroscopy (XAS) has been widely used to elucidate electronic and geometrical information of metals and metal complexes, as the spectra are highly element and state specific.[1,2] Theoretical methods are key tools in understanding the experimental spectra. As X-ray absorption spectroscopy involves core electrons, theoretical methods that incorporate relativistic effects are vitally important for the understanding and prediction of the spectra of even first-row transition metals.

K-edge XAS spectra (excitations from the 1s core level) demonstrate simple scalar relativistic effects, with *ab initio* calculations that neglect scalar relativistic effects red-shifting the absorption spectra compared to experiment.[3–7] L-edge X-ray spectroscopy measures electronic transitions from the $2p$ core orbitals. Like K-edge spectroscopy, L-edge XAS is also element specific, but offers some advantages over K-edge XAS. L-edge spectra have finer linewidths due to longer core-hole life-times, allowing for higher sensitivity. Additionally, spectral features in L-edge XAS are often more intense as transitions are electric dipole allowed. Interpretation and prediction of L-edge spectra is complicated by several factors, including significant relativistic and spin-orbit effects. In addition to scalar relativistic effects affecting the $2s$ and $2p$-orbitals, the spin and orbital angular momentum of an electron in the $2p$-orbital couple, causing a splitting of the $2p$ orbitals into two sets, $2p_{1/2}$ and $2p_{3/2}$, differing in total angular momentum $J$ (1/2 and 3/2 respectively). This results in the X-ray absorption spectra containing two peaks corresponding to excitations from the two sets of $p$ orbitals; these are known as the $L_2$ and $L_3$ edges, with the $L_3$ edge lower in energy. This fundamentally arises from the spin-orbit coupling. *Ab initio* calculations that neglect

spin-orbit coupling predict a single peak. Furthermore, spin-orbit coupling in the $d$ orbitals, ligand field splitting, and charge transfer states result in secondary features and spread the spectra over a range of energy, approximately 20 eV for iron containing systems.

The various theoretical and computational methods used to predict L-edge X-ray spectra have recently been reviewed in detail.[8–11] The most rigorous way of including relativistic effects, spin-orbit coupling, and correlation effect is to solve the Dirac equation in a multi-configurational framework, using either a four-component[12–20] or two-component wavefunction.[21–26] Four-component methods are inherently demanding, therefore much effort has been made to decouple the four-component equations into electron only two-component equation, retaining the key physical relativistic effects of the full four-component equations, but at a reduced computational cost.

In this work, we use the exact two-component X2C method[27–40] to decouple the four-component Dirac-Hartree-Fock into a reduced dimension electronic two-component approach. Relativistic and spin-orbit effects are variationally included at the orbital level in the X2C-Hartree-Fock reference. To account for the multi-configurational behaviour in the ground state of transition metals, we use an X2C state averaged complete active space self consistent field (X2C-SA-CASSCF) method in the Kramers' unrestricted framework.[21,22] The use of multiconfigurational active space for the description of transition metals allows a natural extension to study their X-ray spectra. Using the restricted active space (RAS) formalism,[41,42] excitations can be made from specified core orbitals to the valence space; this has allowed the prediction of various X-ray spectra of transition metals, including K-edge, L-edge and resonance inelastic scattering.[43–51] In this work, we develop an X2C multireference restricted active space configuration interaction (X2C-MRRASCI) approach to predict the L-edge spectra of transition metals complexes.

# 2 Methodology

The X2C-MRRASCI procedure used in this work for predicting the L-edge X-ray absorption spectra of metal complexes can be most broadly split into two steps. Firstly, an accurate description of the ground state of the system is generated using the exact two-component state-averaged CASSCF method,[21] variationally taking into account relativistic and multi-configurational effects. Secondly, this multiconfigurational wavefunction is used as a reference in a two-component X2C-RASCI calculation, where excitation from the core to valence space is allowed, producing an X-ray absorption spectrum.

## 2.1 X2C and Relativistic Effects

As stated above, the most common way to include spin-orbit coupling in active-space methods is to use a perturbative approach such as that defined by Malmqvist *et al*,[52] known as the complete/restricted active space state interaction method (CASSI/RASSI). In this approach, states that may mix with the state of interest under the influence of the spin-orbit operator are computed. These are usually the states with spin multiplicities of $\pm 2$ relative to the state of interest. A spin-orbit Hamiltonian is constructed in the basis of those states.[52,53] This Hamiltonian is then diagonalized to yield a new set of states and energies, which may be further improved by including dynamic correlation corrections. This approach is computationally efficient, in that the wavefunction is both real and one-component in nature. However, the approach relies on Russell-Saunders (LS) coupling of the angular momenta. The LS coupling and the perturbative approach is likely to break down further down the periodic table, where coupling resembles $JJ$-coupling and the magnitude of the spin-orbit coupling increases.[23,54]

Alternatively, spin-orbit coupling (and scalar relativistic effects) can be included variationally during the orbital optimization procedure. In the full-CI limit, the results of the two approaches are the same, but for truncated CI expansions, including spin orbit coupling

in the orbital optimization can capture the $JJ$-coupling like behavior seen lower down the periodic table. Therefore variational inclusion is the paradigm used in the current work, where the X2C transformation is used to include relativistic effects in a two-component state-averaged CASSCF method.[21,22]

In the spinor basis, the matrix representation of the restricted-kinetic-balanced Dirac equation is:[55]

$$\begin{pmatrix} \mathbf{V} & \mathbf{T} \\ \mathbf{T} & \frac{1}{4c^2}\mathbf{W} - \mathbf{T} \end{pmatrix} \begin{pmatrix} \mathbf{C}_L^+ & \mathbf{C}_L^- \\ \mathbf{C}_S^+ & \mathbf{C}_S^- \end{pmatrix} = \begin{pmatrix} \mathbf{S} & \mathbf{0}_2 \\ \mathbf{0}_2 & \frac{1}{2c^2}\mathbf{T} \end{pmatrix} \begin{pmatrix} \mathbf{C}_L^+ & \mathbf{C}_L^- \\ \mathbf{C}_S^+ & \mathbf{C}_S^- \end{pmatrix} \begin{pmatrix} \boldsymbol{\epsilon}^+ & \mathbf{0} \\ \mathbf{0} & \boldsymbol{\epsilon}^- \end{pmatrix} \tag{1}$$

where $c$ is the speed of light. $\mathbf{V}$, $\mathbf{T}$, and $\mathbf{S}$ are the two-component non-relativistic potential energy, kinetic energy, and overlap matrices, respectively. $\mathbf{W}$ is the relativistic potential matrix, defined as $(\vec{\sigma}\cdot\vec{p})\,\mathbf{V}(\vec{\sigma}\cdot\vec{p})$, where $\vec{p}$ is the linear momentum operator and $\vec{\sigma}$ contains Pauli spin matrices. $\{\epsilon^+\}$, $\{\epsilon^-\}$ are the sets of positive/negative eigenvalues with corresponding molecular orbital coefficients $(\mathbf{C}_L^+ \quad \mathbf{C}_S^+)^T$ for the positive and $(\mathbf{C}_L^- \quad \mathbf{C}_S^-)^T$ for the negative energy solutions.

In this work, we use the exact-two-component (X2C)[27–39,56] technique to "fold" the small component coefficients $\mathbf{C}_S^-$ into the large component by a one-step unitary transformation, resulting in an electron-only Hamiltonian (see Ref. 35 for numerical implementations). We use the one-electron X2C approach where the exact transformation of the one-body Hamiltonian is achieved. To lower the computational cost, here we only use the bare Coulomb operator instead of transforming from the four-component two-electron operator. This leads to a Hamiltonian that ignores important two-electron relativistic effects, such as the two-electron spin-orbit. To mitigate the error, we use an empirical factor, known as the Boettger factor,[57] to scale the one-electron spin-orbit terms and mimic the two-electron spin-orbit effects.

The X2C transformation yields a set of spinor molecular orbitals, which are complex

linear combinations of AO spinor orbitals.

$$\psi_p^{2c}(\mathbf{q}) = \begin{pmatrix} \phi_p^{\alpha}(\mathbf{r}) \\ \phi_p^{\beta}(\mathbf{r}) \end{pmatrix} = \begin{pmatrix} \sum_\mu c_{\mu p}^{\alpha} \chi_\mu(\mathbf{r}) \\ \sum_\mu c_{\mu p}^{\beta} \chi_\mu(\mathbf{r}) \end{pmatrix} \tag{2}$$

where coordinate $\mathbf{q}$ includes both the spatial coordinate $\mathbf{r}$ and the spin coordinate. The spatial functions of $\{\phi_p^{\alpha}\}$ and $\{\phi_p^{\beta}\}$ are expanded in a common set of real atomic orbitals $\{\chi_\mu\}$ with complex coefficients.

In this work the ground state of the system is described by a two-component state-averaged CASSCF method using the X2C framework, referred to here as X2C-SA-CASSCF (see Ref. 21). This method has distinct advantages over perturbative approaches. Firstly, spinor molecular orbitals obtained via this procedure include relativistic effects in a variational manner. Secondly, the use of careful state averaging allows the recovery of Kramers symmetry in open-shell cases. State averaging also treats multiple states on an equal footing. These effects combine to allow the description of degenerate multiplets and of low-lying excited states – features common in transition metals.

## 2.2 RASCI and Definition of Sub-Spaces

The X2C-SA-CASSCF wavefunction (orbitals and configurations) is used as a multiconfigurational reference from which to compute the L-edge X-ray absorption spectrum using X2C-RASCI. The two-component MRRASCI used in this work uses the two-component multireference configuration interaction framework developed by the present authors,[22] with the flexibility of the definition of the correlation space allowing the restriction to RASCI (see 22 for details).

In RASCI, configurations are generated subject to certain restrictions on hole or electron occupancy in each sub-space:

- RAS1: number of holes ($i_{\mathrm{h}}$) in this space must be less than the maximum allowed hole

occupancy ($m_\mathrm{h}$);

- RAS2: no restriction, equivalent to a complete active space;
- RAS3: number of electrons ($i_\mathrm{e}$) in this space must be less than the maximum allowed electron occupancy ($m_\mathrm{e}$).

The total number of unique determinants in this two-component RAS framework is

$$N_\mathrm{det} = \sum_{i_\mathrm{h}=0}^{m_\mathrm{h}} \sum_{i_\mathrm{e}=0}^{m_\mathrm{e}} \binom{N_\mathrm{RAS1}}{i_\mathrm{h}} \binom{N_\mathrm{RAS2}}{n_\mathrm{e} - N_\mathrm{RAS1} + i_\mathrm{h} - i_\mathrm{e}} \binom{N_\mathrm{RAS3}}{i_\mathrm{e}} \tag{3}$$

where $N_\mathrm{RAS1}$, $N_\mathrm{RAS2}$, $N_\mathrm{RAS3}$ are the numbers of orbitals in RAS1, RAS2/CAS, RAS3 spaces and $n_e$ is the total number of electrons in the correlated space. Note that the RASCI framework does not enforce Kramers symmetry. Due to the use of two-component spinor molecular orbitals, the configurations generated have varied spin multiplicities.

## 2.3 Active Spaces for $L_{2,3}$ Spectra

The $L_{2,3}$ spectrum of first row transition metal complexes involves the excitation of an electron from the $2p$ to low-lying unoccupied orbitals. Therefore, the computational description of this process using RASCI places the $2p$ orbitals in the RAS1 space and the low-lying unoccupied orbitals are placed in the RAS2 active space. A single excitation from RAS1 is then allowed (*i.e.*, $m_h = 1$). The calculations presented in this work do not contain a RAS3 space, unless stated otherwise. This simple partitioning may be used as a first approximation. For systems where dynamic correlation is more significant, the correlation space can be systematically expanded to include higher-energy virtual orbitals in RAS3, and if necessary, fully occupied orbitals in RAS1; both the size of correlation space and level of excitation are fully variable within the RASCI formalism used here.[22] For XAS calculations, the well-known $d$ double-shell effect[58,59] has been shown to only have a small effect on the spectrum.[45] Accordingly, only one set of $d$ orbitals may be included in the active space without significant

loss in accuracy.

## 2.4 Spectral Intensity

The eigenvalues of the X2C-MRRASCI Hamiltonian matrix determine the energies of the excited states, *i.e.*, the peak position in the L-edge spectrum. We now define how to calculate the intensity of each transition. As stated above, the transition probabilities for L-edge spectra are electric dipole-allowed. Using the MO-dipole integrals, $d^{\omega}$, for the Cartesian directions $\omega = \{x, y, z\}$, the oscillator strength for a transition between states 0 and $n$ can be evaluated (within the dipole approximation)

$$\gamma_{pq}^{0n} = (C_I^0)^* \, \langle I|E_{pq}|J\rangle \, C_J^n \tag{4}$$

$$D^{\omega,0n} = \left(\sum_{p,q} \gamma_{pq}^{0n}.d_{qp}^{\omega}\right).\left(\sum_{p,q} \gamma_{pq}^{n0}.d_{qp}^{\omega}\right) \tag{5}$$

$$|\mu^2| = D^{x,0n} + D^{y,0n} + D^{z,0n} \tag{6}$$

$$f = \frac{2}{3}|\mu^2|.\Big(E_n - E_0\Big) \tag{7}$$

where $\hat{E}_{pq}$ is a single excitation operator, $|I\rangle, |J\rangle$ indicate determinants, $C_J^n$ the coefficient of determinant $|J\rangle$ in state $n$ and $E_n$ the energy of state $n$. As the systems presented here have degenerate ground states, the oscillator strength is computed from each ground state and summed to give a total oscillator strength.

With the peak position and relative intensity determined, the spectrum is adjusted to account for both lifetime and experimental broadening. A Voigt convolution of a Lorentzian and a Gaussian is used. The Gaussian parameters are chosen to match the width of the main $L_3$ feature and represent broadening due to experimental resolution. Due to the difference in core-hole lifetimes between $p_{1/2}$ and $p_{3/2}$, separate Lorentzian broadening is applied to the $L_3$ and $L_2$ edges. A point equi-distance between the $L_3$ and $L_2$ edges separates the broadening regions. The total intensity is scaled such that the most intense $L_3$ peak has an intensity of

1.0. In addition, the computed spectrum is uniformly shifted to match the position of the most intense experimental peak. shift is dependent on the specific active space and basis set used, but for the examples presented here lies in the range 11-15 eV. The character of the computed peaks can be determined from the X2C-MRRASCI density matrices for specific states and can be compared to any assigned peaks in the experimental spectrum. This aids in determining and validating the global shift but also allows analysis and understanding of the experimental spectrum.

# 3 Results and Discussion

The combined X2C-SA-CASSCF and X2C-RASCI (X2C-MRRASCI) procedure defined above is benchmarked for the calculation of $L_{2,3}$-edge spectra of iron complexes. These methods are implemented in a local development version of the Gaussian software package,[60] which is used in all calculations presented.

## 3.1 $Fe^{3+}$

The benchmark calculations presented here focus on L-edge spectra of iron complexes. Therefore it is appropriate to first assess the performance of the X2C-MRRASCI procedure on the free ion $Fe^{3+}$. The high spin ground state of $Fe^{3+}$ is a six-fold degenerate $^6S_{5/2}$ state. These degenerate ground states can be described using X2C-SA-CASSCF, with an active space comprised of the d orbitals (5 electrons in 10 spinor orbitals) and state-averaging over the six states. This recovers the degeneracy of the states to within the energy convergence criteria. In order to compute the L-edge spectrum, a subsequent X2C-RASCI calculation is performed, using the *d* orbitals as the RAS2 space and the 2*p* orbitals as the RAS1 space, and allowing single excitations from RAS1. The computed spectrum, using a Sapporo-DKH3-DZP-2012 basis with diffuse functions,[61] is shown in Fig. 1.

The exact character of each peak of the spectrum has been analysed and discussed in

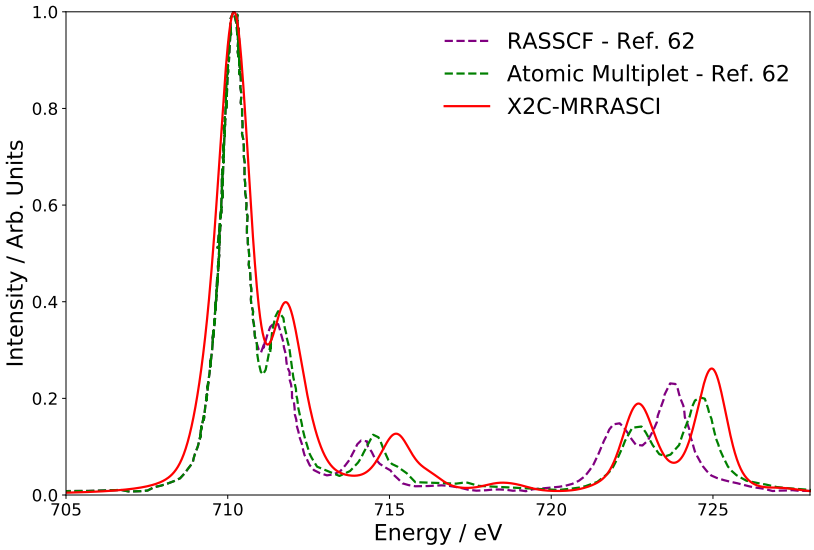


**Figure 1.** The $L_{2,3}$ edge of the XAS spectrum of $Fe^{3+}$ computed using the X2C-MRRASCI procedure and compared to both the perturbative RASSI-RASSCF approach and semi-empirical atomic multiplet calculations of Pinjari *et al.*,[62] reprinted from Pinjari, R. V.; Delcey, M. G.; Guo, M.; Odelius, M.; Lundberg, M. *Journal of Chemical Physics*, 2015, vol. 142, page 069901 with the permission of AIP Publishing. The computed spectra are shifted to align the most intense peak, and Voigt broadening applied.

detail.[45,62] As expected, the most intense feature arises from $2p_{3/2} \rightarrow d$ orbitals, with shoulder peaks corresponding to different occupations of the $d$ orbitals that are split by $d$ orbital spin orbit coupling, this is the $L_3$ region. The $L_2$ region, >720eV, corresponds to $2p_{1/2} \rightarrow d$. The spectrum computed using X2C-MRRASCI shows good agreement with literature predictions of the L-edge spectrum using RASSI-RASSCF and atomic multiplet calculations,[62] and agrees with the character assigned in Ref. 62. The three methods agree on the main features of the spectrum, but differ slightly in the relative energy spacing of the peaks. This difference in spacing is most obvious for the gap between the $L_3$ and $L_2$ regions, a direct result of the magnitude of the spin-orbit coupling in the $2p$ orbitals, with the energy gap being larger in X2C-MRRASCI.

## 3.2 $\left[\mathbf{Fe(H_2O)_6}\right]^{2+}$

Core excitation of $\left[\mathrm{Fe(H_2O)_6}\right]^{2+}$ and related systems have been the subject of both experimental and theoretical studies,[48,63–66] including induced core-hole ultrafast spin dynamics.[63] Various theoretical methods have been used to study the geometries of $\left[\mathrm{Fe(H_2O)_6}\right]^{2+}$.[67,68] For the high-spin case, a slight distortion from $D_{4h}$ symmetry is suggested, but estimates of bond lengths differ. As this system is used here to demonstrate the utility of the X2C-MRRASCI approach, rather than exactly quantify the experimental spectrum, we simplify the geometry to that of a model system. Here, for simplicity, we model an octahedral arrangement of oxygen atoms around a central iron, and optimize other degrees of freedom using B3LYP/6-31G(d), giving a predicted iron-oxygen bond length of 2.002Å, and ignore solvent effects present in experiment.

The electronic configuration of iron in this system is Fe(II)-$d^6$. This corresponds to a free ion ground state term of $^5$D, which comprises 25 microstates. The introduction of spin-orbit coupling splits these states into the $J = 4, 3, 2, 1, 0$ sets, with $J = 4$ being the lowest in energy, forming the 9-tuply degenerate ground state. Embedding of this in the weak octahedral oxygen ligand field splits the ground states into $T_2$, E, $T_1$ and $A_1$, as shown in Tab. 1 (further details are provided in Ref. 69 and 70).

**Table 1.** Splitting of Fe(II)-$d^6$ upon the inclusion of spin-orbit and ligand field effects in octahedral $\left[\mathrm{Fe(H_2O)_6}\right]^{2+}$.

| $SO_3$ | Total Symmetry in $O_h$ |
|---|---|
| $^5D_0$ J = 0 | $A_1$ |
| $^5D_1$ J = 1 | $T_1$ |
| $^5D_2$ J = 2 | E |
| | $T_2$ |
| $^5D_3$ J = 3 | $A_2$ |
| | $T_2$ |
| | $T_1$ |
| $^5D_4$ J = 4 | $A_1$ |
| | $T_1$ |
| | E |
| | $T_2$ |

In order to describe the ground state electronic structure of this system, including both

**Table 2.** Formally triply-degenerate $T_2$ ground state of $\left[Fe(H_2O)_6\right]^{2+}$ as computed using X2C-SA-CASSCF, state averaging equally over 25 states and the X2C-TZVPall-2c basis set.[71]

| | Energy (a.u.) |
|---|---|
| $T_2$ | −1727.64320260 |
| | −1727.64320260 |
| | −1727.64320260 |

ligand field and spin-orbit effects, X2C-SA-CASSCF is used with an active space comprised of the $d$ orbitals ($t_{2g}$ and $e_g$ in the octahedral ligand field), state averaging over the 25 states arising from the splitting of the $^5$D term. This correctly reproduces the sets of states seen in Tab. 1, with correct degeneracy, as demonstrated for the triply-degenerate $T_2$ ground state in Tab. 2.

The second step to compute the L-edge spectrum is the X2C-MRRASCI calculation. The iron $2p$-orbitals are included RAS1, while the $d$-orbitals comprise RAS2 ($t_{2g}$ and $e_g$ in the ligand field). As stated in the Methodology section, the number of holes in RAS1 is restricted to be a maximum of 1, generating a set of RASCI configurations that include all $((2p)^5,(3d)^7)$ permutations. The computed $L_{2,3}$ edge spectrum is compared to experiment in Fig. 2.

The main features of the spectrum are reproduced by X2C-MRRASCI – the main $L_3$ peak at ∼708 eV, and satellite peaks at 709-714 eV. Each edge contains a lower energy region corresponding to $p \rightarrow t_{2g}$ transition, a higher energy region corresponding to $p \rightarrow e_g$ and an intermediate region comprised of a mix of multiplets involving excitation to both. Within a single particle model, the $L_3 : L_2$ intensity ratio is 2:1. This is affected by electron correlation and spin-orbit coupling of the $3d$ orbitals. Here the intensity ratio $L_3/L_2$ is reproduced nearly exactly, showing the key effects are captured by X2C-MRRASCI. The positions of the $L_2$ peaks are reproduced but the two lower energy peaks of $L_2$, dominated by $p_{1/2} \rightarrow t_{2g}$ transitions, are shifted higher in energy compared to experiment. The relative positions of the $L_3$ and $L_2$ regions is related to the magnitude of the spin-orbit coupling in the $p$ orbitals. The positions of the peaks in the high-$L_2$ region, at 723-725 eV, compare

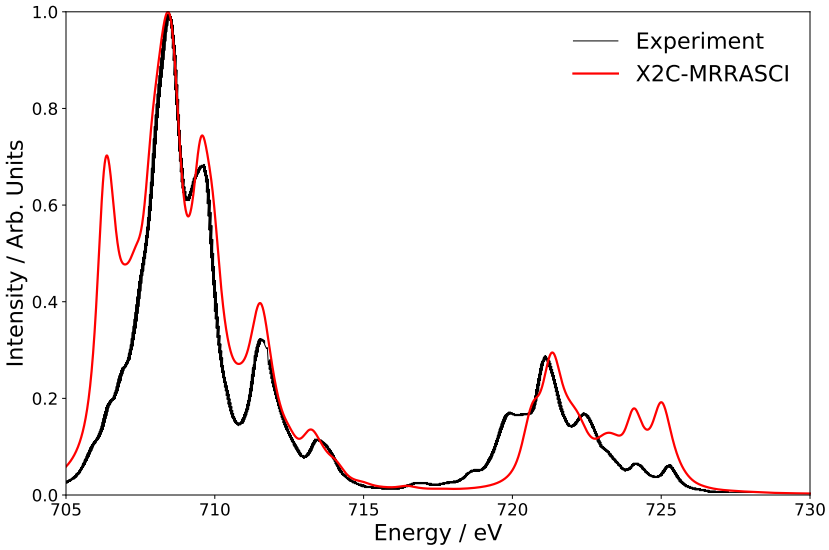


**Figure 2.** Comparison of the predicted and experimental[63] $L_{2,3}$ edge of the XAS spectrum of $\left[Fe(H_2O)_6\right]^{2+}$. The computed spectrum is shifted to align the most intense peak with experiment, and Voigt broadening applied. Experimental data adapted with permission from Ref. 63, copyrighted by the American Physical Society.

well to experiment, showing the magnitude of the spin-orbit coupling is accurately predicted. The lower-$L_2$ region, at 720-723 eV, shows a relative shift in the peak positions. This shift is likely not due to errors in spin-orbit coupling, but a result of the small active space affecting the low energy region. Separation of lower-$L_2$ peaks may be improved by enlarging the active space, particularly including $3p$-$3d$ correlation, which has been shown to be important for the relative energies of the initial states of $3d$ atoms.[72]

The relative intensity of the peaks generally follow experiment, with the exception of the intensity of the low energy peak at approximately 706 eV (dominated by $p_{3/2} \rightarrow t_{2g}$ occupied states); this intensity is overestimated by X2C-MRRASCI. This peak arises from numerous states with various $t_{2g}$ and $e_g$ occupation, making the exact cause difficult to ascertain.

## 3.3 $FeCl_4^-$

In this section, X2C-MRRASCI is used to compute the L-edge X-ray absorption spectrum of $FeCl_4^-$. In this molecule, the iron has an electronic configuration of Fe(III) $- d^5$. The $^6$S ground state of a free ion splits in the tetrahedral ligand field of the Cl atoms to yield a $^6A_1$ ground state with an orbital occupancy of $e^2t_2^3$. The introduction of spin-orbit coupling further splits this into $E_{5/2}$ and $G_{3/2}$ states. Here, these lowest lying states are described by X2C-SA-CASSCF using 5 electrons in 10 spinor orbitals. As the $E_{5/2}$ and $G_{3/2}$ multiplets are degenerate within the accuracy requested here, state averaging over the 6 states of these multiplets is used.

In order to compute the absorption spectrum, the X2C-SA-CASSCF is used as a reference for X2C-RASCI computations. The X2C-SA-CASSCF active space is used as the RAS2 space, while the iron $2p$ orbitals and electrons comprise the RAS1 space. The computed spectrum is compared to the experimental spectrum[73] of $[Fe^{III}Cl_4](Et_4N)$ in Fig. 3.

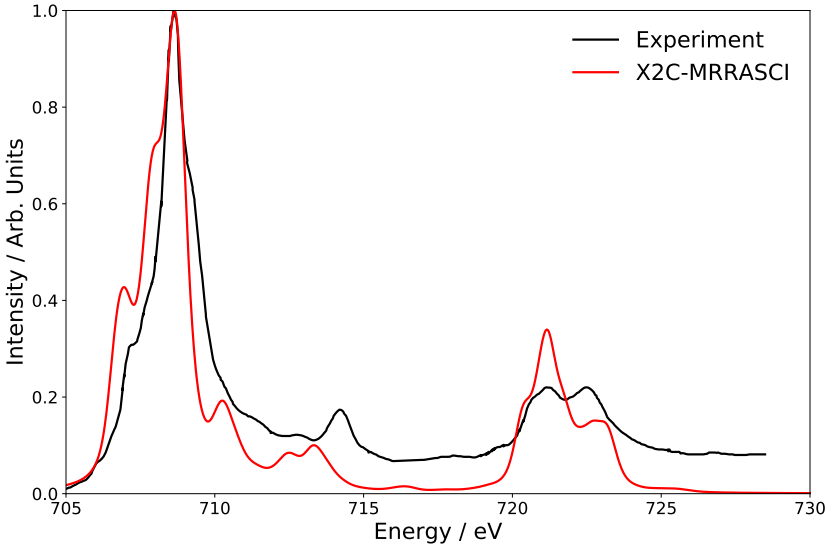


**Figure 3.** Comparison of the predicted and experimental[73] $L_{2,3}$ edge of the XAS spectrum of $FeCl_4^-$. The computed spectrum is shifted to align the most intense peak with experiment, and Voigt broadening applied. An ANO triple-zeta basis is used.[74,75] Experimental data adapted with permission from Ref. 73, copyright 2017 American Chemical Society.

In the computed spectrum, the relative positions of the peaks are reproduced; satellite peaks from 710 to 715 eV, two peaks in $L_2$. However, the intensity of the peak at 706 eV is overestimated. This peak corresponds to a transition from $p_{3/2}$ to a state of mixed $e$ and $t_2$ occupation. This overestimation of the low-energy intensity is similar to that seen in previous example of $\left[Fe(H_2O)_6\right]^{2+}$. Likewise, the corresponding region in $L_2$ is also overestimated. However, the solvent effects present in experiment are not included in the current work, and remain as a possible source of variation between theory and experiment.

## 3.4 $FeCl_6^{3-}$

In this section we test the X2C-MRRASCI method for the computation of the L-edge spectrum of $FeCl_6^{3-}$, a system that has been studied both experimentally[76] and theoretically.[45–47,49] Furthermore, we investigate the effect of the RAS spaces on the result. In order to do this, we must fist understand the molecular orbitals. The bonding molecular orbitals of $FeCl_6^{3-}$ arise by ligand $\sigma$ orbitals (symmetry adapted linear combination of $p$ orbitals) mixing with Fe $3d$ orbitals to form bonding $\sigma$ (and antibonding $\sigma^*$) orbitals of $e_g$ symmetry. Additionally, weak bonding and anti-bonding orbitals are formed from the mixing of Fe $t_{2g}$ orbitals with the $t_{2g}(\pi)$ orbitals formed from the ligand $p$ orbitals.

The ground state of octahedral $FeCl_6^{3-}$ has a high spin electron configuration of $t_{2g}^3 e_g^2$. This gives a $^6A_g$ ground state. This degenerate ground state can be described by X2C-CASSCF using 5 electrons in the $t_{2g}$ and $e_g^2$ orbitals, state averaging over the six degenerate micro-states of $^6A_g$. This correctly gives six degenerate states, *i.e.*, a qualitatively correct set of states, using a minimal active space. These states are then used as a reference for the X2C-RASCI calculation of the L-edge spectrum.

In the molecular system, the L-edge spectrum corresponds to excitation from the $p_{1/2}$ and $p_{3/2}$ orbitals (of $t_{1u}$ symmetry) to $t_{2g}$ and $e_g$ orbitals. Accordingly, the $t_{1u}$ orbitals are included in the RAS1 space. The simplest RAS2 space, space A (shown in Fig. 4, is the same as the CAS space used in the orbital optimization and comprises 5 electrons in 10 orbitals

(6 $t_{2g}$ and 4 $e_g$).

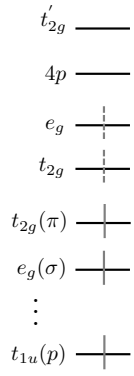


| | A | B | C | D |
|---|---|---|---|---|
| RAS3 | - | - | $t'_{2g}$ | - |
| RAS2 | $t_{2g}$, $e_g$ | $t_{2g}$, $e_g$, $e_g(\sigma)$ | $t_{2g}$, $e_g$, $e_g(\sigma)$ | $t_{2g}$, $e_g$, $e_g(\sigma)$, $t'_{2g}$ |
| RAS1 | $t_{1u}(p)$ | $t_{1u}(p)$ | $t_{1u}(p)$ | $t_{1u}(p)$ |

**Figure 4.** (**top**) Partial molecular orbital diagram for $FeCl_6^{3-}$. Orbitals fully occupied in the ground state are indicated by a solid line, while partial occupation is indicated by a dashed line. (**bottom**) Definition of the different RAS spaces (spaces A-D) used in the X2C-MRRASCI calculation on high spin $FeCl_6^{3-}$. All calculations use the same RAS1 space but differ in the composition of RAS2 and RAS3.

**Table 3.** Dimensions of the X2C-RASCI calculations on $FeCl_6^{3-}$. For each active space defined in Fig. 4, the number of electrons and spinor orbitals in each RAS sub-space is shown (*(electrons, orbitals)*). The resulting total number of determinants generated from these active spaces in X2C-RASCI is indicated in the 3rd column. The number of X2C-RASCI states actually computed, using an energy-specific Davidson procedure, for the $L_{2,3}$ spectrum in Fig. 5 is also given.

| | RAS1 | RAS2 | RAS3 | Determinants | States Computed |
|---|---|---|---|---|---|
| A | (6,6) | (5,10) | - | 1512 | 900 |
| B | (6,6) | (9,14) | - | 8008 | 2500 |
| C | (6,6) | (9,14) | (0,6) | 419848 | 2000 (partial spectrum) |

The computed L-edge spectrum is shown in comparison to experiment in Fig. 5. The results demonstrate that X2C-MRRASCI using only a limited active space satisfactorily reproduces the main experimental features of the spectrum. The experimental spectrum clearly shows the characteristic L-edge features but also shows a peak at $\sim$ 714 eV which has been assigned as a shake-up peak, corresponding to a $2p \rightarrow 3d$ transition coupled to a $\sigma \rightarrow 3d$ ligand-metal-charge-transfer (LMCT).[46,76] This peak is not captured by calculation

using space A, because excitation of the relevant $\sigma$ orbitals is not allowed (they are not present in the active space).

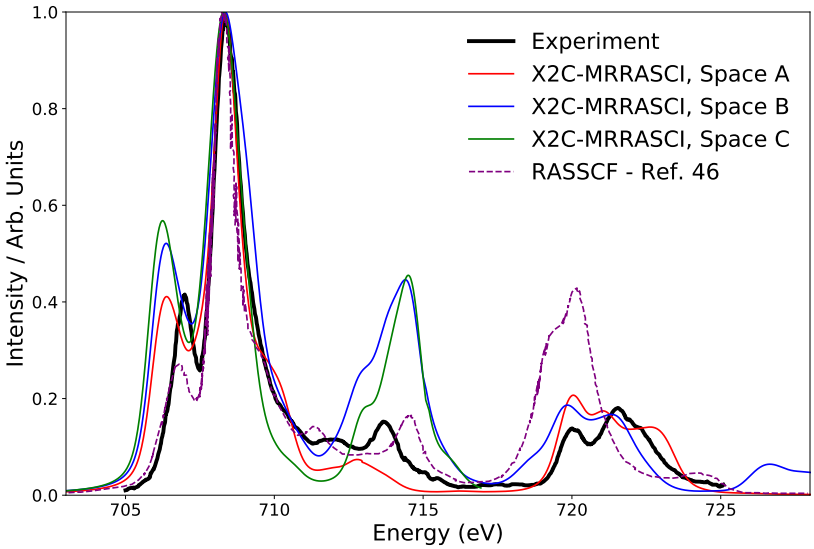


**Figure 5.** Comparison of the predicted and experimental $L_{2,3}$ edge of the XAS spectrum of $FeCl_6^{3-}$, using different active spaces A-C and an ANO triple-zeta basis[74,75](note that the spectrum using Space C is not computed beyond 717 eV). Computed spectra have been broadened and shifted (see main text). Also shown is the perturbative RASSI-RASSCF spectrum of Pinjari *et al.*[46] that use space 'D' in Fig. 4 (see Ref. 46 for details). RASSI-RASSCF spectrum reprinted with permission from Pinjari, R. V.; Delcey, M. G.; Guo, M.; Odelius, M.; Lundberg, M. *Journal of Computational Chemistry*, vol 37, page 477, copyright 2016 Wiley publishing. Experimental data adapted with permission from Ref. 76, copyright 2003 American Chemical Society.

In order to resolve the shake-up peak, the active space used was expanded. In space B, shown in Fig. 4, the $\sigma$ orbitals are included. The computed spectrum, shown in Fig. 5, overestimates the overall intensity across the energy range, but importantly, shows the emergence of the LMCT peak when the $\sigma$ orbitals are included. Furthermore, inclusion of the $\sigma$ orbitals also gives rise to a higher energy satellite peak of the $L_2$ edge, a peak also predicted by Pinjari *et al.*,[46] but not seen in the experimental data.

X2C-MRRASCI calculations using space B over-estimate the intensity of the shake-up peak compared to both experiment and the RASSI-RASSCF calculations of Pinjari *et al.*[46] To investigate the source of this over-estimation, the $t_{2g}^{'}$ orbitals identified to play an im-

portant role in correlation[45,46] have been included in RAS3 to act as correlating orbitals (see space 'C' in Fig. 4). However, the computed spectrum changes very little (see Fig. 5), showing the same over-estimation of the shake-up peak compared to experiment and RASSI-RASSCF. This suggests that orbital relaxation effects, as allowed in the RASSI-RASSCF calculations of Ref. 46, may be more important for describing this shake-up peak.

# 4 Conclusion

In this work we present X2C-MRRASCI, a combined X2C-SA-CASSCF and X2C-RASCI approach for the computation of L-edge X-ray absorption spectra. This approach allows for variational inclusions of relativistic effects and spin-orbit couplings at the molecular orbital level. The procedure is benchmarked for the L-edge spectra of iron complexes.

Results show that even with a minimal active space, key features of the absorption spectrum are captured. Although two-electron spin-orbit coupling is only approximated using an empirical scaling of the one-electron coupling, results show accurate separation of the $L_3$ and $L_2$ edges.

The use of small active spaces leads to a lack of dynamic correlation, which is likely to affect the relative intensities of the peaks in the systems we have studied but not the qualitative features, which are the focus of this work. Careful studies using larger active spaces are likely to resolve the overestimation of the intensity of low-energy transitions seen in each spectrum. Similar studies have already shown the significant effects of expanding the active space and adding perturbative corrections for dynamic correlation, particularly on the $L_2$ edge.[46,47] However, the calculations on $FeCl_6^{3-}$ presented here do not suffer from large over-estimation of the intensities of the $L_2$ edge but rather over-estimate the shake-up peak. Expanding the active space to account for leading dynamic correlations, and to allow easier comparison to literature, shows little improvement over existing spaces used, suggesting orbital relaxation after core-excitation, as allowed in the RASSCF calculations

of Ref. 46, may play an important role in the prediction of accurate intensities for these transitions. This effect warrants further development and investigation.

Perturbative spin-orbit coupling approaches have shown similar performance for early transition metals, however, a variational approach is likely to vital as the magnitude of the spin-orbit coupling is increased, for example, as one studies elements further down the periodic table. Through careful choice of the RAS spaces, the X2C-MRRASCI method detailed here may be used for further X-ray absorption studies, including M-edge, providing a useful analysis and predictive tool.

# Acknowledgement

X. L. acknowledges support from the U.S. Department of Energy (DOE), Office of Science, Basic Energy Sciences, in the Heavy-Element Chemistry program (Grant No. DE-SC0021100) for the development of electronic structure methods within the four-component Dirac framework, and the Computational and Theoretical Chemistry program (Grant No. DE-SC0006863) for studies of L-edge spectroscopy.

# References


(1) de Groot, F.; Kotani, A. *Core Level Spectroscopy of Solids*; CRC Press, 2008.

(2) Norman, P.; Dreuw, A. Simulating X-ray Spectroscopies and Calculating Core-Excited States of Molecules. *Chem. Rev.* **2018**, *118*, 7208–7248.

(3) DeBeer George, S.; Petrenko, T.; Neese, F. Time-dependent Density Functional Calculations of Ligand K-edge X-ray Absorption Spectra. *Inorg. Chim. Acta* **2008**, *361*, 965–972.

(4) Lestrange, P. J.; Nguyen, P. D.; Li, X. Calibration of Energy-Specific TDDFT for Modeling K-Edge XAS Spectra of Light Elements. *J. Chem. Theory Comput.* **2015**, *11*, 2994–2999.

(5) Peng, B.; Lestrange, P. J.; Goings, J. J.; Caricato, M.; Li, X. Energy-Specific Equation-of-Motion Coupled-Cluster Methods for High-Energy Excited States: Application to K-Edge X-Ray Absorption Spectroscopy. *J. Chem. Theory Comput.* **2015**, *11*, 4146–4153.

(6) Fronzoni, G.; De Francesco, R.; Stener, M. Time Dependent Density Functional Theory of X-ray Absorption Spectroscopy of Alkaline-Earth Oxides. *J. Phys. Chem. B* **2005**, *109*, 10332–10340.

(7) Besley, N. A.; Asmuruf, F. A. Time-dependent Density Functional Theory Calculations of the Spectroscopy of Core Electrons. *Phys. Chem. Chem. Phys.* **2010**, *12*, 12024–12039.

(8) Kasper, J. M.; Stetina, T. F.; Jenkins, A. J.; Li, X. Ab Initio Methods for L-edge X-ray Absorption Spectroscopy. *Chem. Phys. Rev.* **2020**, *1*, 011304.

(9) Besley, N. A. Modeling of the Spectroscopy of Core Electrons With Density Functional Theory. *WIREs Comput. Mol. Sci.* **2021**, *11*, 1527.

(10) Besley, N. A. Density Functional Theory Calculations of Core–Electron Binding Energies at the K-Edge of Heavier Elements. *J. Chem. Theory Comput.* **2021**, *17*, 3644–3651.

(11) Vidal, M. L.; Pokhilko, P.; Krylov, A. I.; Coriani, S. Equation-of-Motion Coupled-Cluster Theory to Model L-Edge X-ray Absorption and Photoelectron Spectra. *J. Phys. Chem. Lett.* **2020**, *11*, 8314–8321.

(12) Jensen, H. J. A.; Dyall, K. G.; Saue, T.; Fægri, K. Relativistic Four-component Multiconfigurational Self-Consistent-Field Theory for Molecules: Formalism. *J. Chem. Phys.* **1996**, *104*, 4083–4097.

(13) Thyssen, J.; Fleig, T.; Jensen, H. J. A. A Direct Relativistic Four-component Multiconfiguration Self-Consistent-Field Method for Molecules. *J. Chem. Phys.* **2008**, *129*, 034109.

(14) Almoukhalalati, A.; Knecht, S.; Jensen, H. J. A.; Dyall, K. G.; Saue, T. Electron Correlation within the Relativistic No-pair Approximation. *J. Chem. Phys.* **2016**, *145*, 074104.

(15) Shiozaki, T.; Mizukami, W. Relativistic Internally Contracted Multireference Electron Correlation Methods. *J. Chem. Theory Comput.* **2015**, *11*, 4733–4739.

(16) Bates, J. E.; Shiozaki, T. Fully Relativistic Complete Active Space Self-Consistent Field for Large Molecules: Quasi-second-order Minimax Optimization. *J. Chem. Phys.* **2015**, *142*, 044112.

(17) Bagus, P. S.; Nelin, C. J.; Ilton, E. S.; Sassi, M. J.; Rosso, K. M. Analysis of X-Ray Adsorption Edges: $L_{2,3}$ Edge of $FeCl_4^-$. *J. Chem. Phys.* **2017**, *147*, 224306.

(18) Knecht, S.; Legeza, O.; Reiher, M. Communication: Four-component Density Matrix Renormalization Group. *J. Chem. Phys.* **2014**, *140*, 041101.

(19) Battaglia, S.; Keller, S.; Knecht, S. Efficient Relativistic Density-Matrix Renormalization Group Implementation in a Matrix-Product Formulation. *J. Chem. Theory Comput.* **2018**, *14*, 2353–2369.

(20) Halbert, L.; Vidal, M. L.; Shee, A.; Coriani, S.; Severo Pereira Gomes, A. Relativistic EOM-CCSD for Core-Excited and Core-Ionized State Energies Based on the Four-Component Dirac–Coulomb(Gaunt) Hamiltonian. *J. Chem. Theory Comput.* **2021**, *17*, 3583–3598.

(21) Jenkins, A. J.; Liu, H.; Kasper, J. M.; Frisch, M. J.; Li, X. Variational Relativistic Complete Active Space Self-Consistent Field Method. *J. Chem. Theory Comput.* **2019**, *15*, 2974–2982.

(22) Hu, H.; Jenkins, A. J.; Liu, H.; Kasper, J. M.; Frisch, M. J.; Li, X. Relativistic Two-Component Multireference Configuration Interaction Method with Tunable Correlation Space. *J. Chem. Theory Comput.* **2020**, *16*, 2975–2984.

(23) Knecht, S.; Jensen, H. J. A.; Saue, T. Relativistic Quantum Chemical Calculations Show That the Uranium Molecule $U_2$ Has a Quadruple Bond. *Nat. Chem.* **2019**, *11*, 40–44.

(24) Fleig, T.; Marian, C. M.; Olsen, J. Spinor Optimization for a Relativistic Spin-Dependent CASSCF Program. *Theor. Chem. Acc.* **1997**, *97*, 125–135.

(25) Kim, I.; Lee, Y. S. Two-component Kramers Restricted Complete Active Space Self-Consistent Field Method with Relativistic Effective Core Potential Revisited: Theory, Implementation, and Applications to Spin-Orbit Splitting of Lower p-Block Atoms. *J. Chem. Phys.* **2013**, *139*, 134115.

(26) Kim, Y. S.; Lee, Y. S. The Kramers' Restricted Complete Active Space Self-Consistent-Field Method for Two-Component Molecular Spinors and Relativistic Effective Core Potentials Including Spin–Orbit Interactions. *J. Chem. Phys.* **2003**, *119*, 12169–12178.

(27) Kutzlenigg, W.; Liu, W. Quasirelativistic Theory Equivalent to Fully Relativistic Theory. *J. Chem. Phys.* **2005**, *123*, 241102.

(28) Liu, W.; Peng, D. Infinite-Order Quasirelativistic Density Functional Method Based on the Exact Matrix Quasirelativistic Theory. *J. Chem. Phys.* **2006**, *125*, 044102.

(29) Peng, D.; Liu, W.; Xiao, Y.; Cheng, L. Making Four- and Two-Component Relativistic Density Functional Methods Fully Equivalent Based on the Idea of From Atoms to Molecule. *J. Chem. Phys.* **2007**, *127*, 104106.

(30) Ilias, M.; Saue, T. An Infinite-Order Relativistic Hamiltonian by a Simple One-Step Transformation. *J. Chem. Phys.* **2007**, *126*, 064102.

(31) Liu, W.; Peng, D. Exact Two-component Hamiltonians Revisited. *J. Chem. Phys.* **2009**, *131*, 031104.

(32) Liu, W. Ideas of Relativistic Quantum Chemistry. *Mol. Phys.* **2010**, *108*, 1679–1706.

(33) Saue, T. Relativistic Hamiltonians for Chemistry: A Primer. *ChemPhysChem* **2011**, *12*, 3077–3094.

(34) Li, Z.; Xiao, Y.; Liu, W. On the Spin Separation of Algebraic Two-Component Relativistic Hamiltonians. *J. Chem. Phys.* **2012**, *137*, 154114.

(35) Peng, D.; Middendorf, N.; Weigend, F.; Reiher, M. An Efficient Implementation of Two-Component Relativistic Exact-Decoupling Methods for Large Molecules. *J. Chem. Phys.* **2013**, *138*, 184105.

(36) Egidi, F.; Goings, J. J.; Frisch, M. J.; Li, X. Direct Atomic-Orbital-Based Relativistic Two-Component Linear Response Method for Calculating Excited-State Fine Structures. *J. Chem. Theory Comput.* **2016**, *12*, 3711–3718.

(37) Goings, J. J.; Kasper, J. M.; Egidi, F.; Sun, S.; Li, X. Real Time Propagation of the Exact Two Component Time-Dependent Density Functional Theory. *J. Chem. Phys.* **2016**, *145*, 104107.

(38) Konecny, L.; Kadek, M.; Komorovsky, S.; Malkina, O. L.; Ruud, K.; Repisky, M. Acceleration of Relativistic Electron Dynamics by Means of X2C Transformation: Application to the Calculation of Nonlinear Optical Properties. *J. Chem. Theory Comput.* **2016**, *12*, 5823–5833.

(39) Egidi, F.; Sun, S.; Goings, J. J.; Scalmani, G.; Frisch, M. J.; Li, X. Two-Component Non-Collinear Time-Dependent Spin Density Functional Theory for Excited State Calculations. *J. Chem. Theory Comput.* **2017**, *13*, 2591–2603.

(40) Liu, J.; Cheng, L. Relativistic Coupled-Cluster and Equation-of-Motion Coupled-Cluster Methods. *WIREs Comput. Mol. Sci.* **2021**, *11*, 1536.

(41) Olsen, J.; Roos, B. O.; Jørgensen, P.; Jensen, H. J. A. Determinant Based Configuration Interaction Algorithms for Complete and Restricted Configuration Interaction Spaces. *J. Chem. Phys.* **1988**, *89*, 2185–2192.

(42) Malmqvist, P. Å.; Rendell, A.; Roos, B. O. The Restricted Active Space Self-consistent-field Method, Implemented with a Split Graph Unitary Group Approach. *J. Phys. Chem.* **1990**, *94*, 5477–5482.

(43) Engel, N.; Bokarev, S. I.; Suljoti, E.; Garcia-Diez, R.; Lange, K. M.; Atak, K.; Golnak, R.; Kothe, A.; Dantz, M.; Kühn, O.; Aziz, E. F. Chemical Bonding in Aqueous Ferrocyanide: Experimental and Theoretical X-ray Spectroscopic Study. *J. Phys. Chem. B* **2014**, *118*, 1555–1563.

(44) Guo, M.; Sørensen, L. K.; Delcey, M. G.; Pinjari, R. V.; Lundberg, M. Simulations of Iron K Pre-edge X-ray Absorption Spectra Using the Restricted Active Space Method. *Phys. Chem. Chem. Phys.* **2016**, *18*, 3250–3259.

(45) Pinjari, R. V.; Delcey, M. G.; Guo, M.; Odelius, M.; Lundberg, M. Restricted Active Space Calculations of L-edge X-ray Absorption Spectra: From Molecular Orbitals to Multiplet States. *J. Chem. Phys.* **2014**, *141*, 124116.

(46) Pinjari, R. V.; Delcey, M. G.; Guo, M.; Odelius, M.; Lundberg, M. Cost and Sensitivity of Restricted Active-space Calculations of Metal L-edge X-ray Absorption Spectra. *J. Comput. Chem.* **2016**, *37*, 477–486.

(47) Delcey, M. G.; Sørensen, L. K.; Vacher, M.; Couto, R. C.; Lundberg, M. Efficient Calculations of a Large Number of Highly Excited States for Multiconfigurational Wavefunctions. *J. Comput. Chem.* **2019**, *40*, 1789—-1799.

(48) Bokarev, S. I.; Dantz, M.; Suljoti, E.; Kühn, O.; Aziz, E. F. State-dependent electron delocalization dynamics at the solute-solvent interface: Soft-x-ray absorption spectroscopy and Ab initio calculations. *Physical Review Letters* **2013**, *111*, 083002.

(49) Lundberg, M.; Delcey, M. G. In *Transition Metals in Coordination Environments: Computational Chemistry and Catalysis Viewpoints*; Broclawik, E., Borowski, T., Radoń, M., Eds.; Springer International Publishing: Cham, 2019; pp 185–217.

(50) Josefsson, I.; Kunnus, K.; Schreck, S.; Föhlisch, A.; de Groot, F.; Wernet, P.; Odelius, M. Ab Initio Calculations of X-ray Spectra: Atomic Multiplet and Molecular Orbital Effects in a Multiconfigurational SCF Approach to the L-Edge Spectra of Transition Metal Complexes. *J. Phys. Chem. Lett.* **2012**, *3*, 3565–3570.

(51) Carreras, A.; Jiang, H.; Pokhilko, P.; Krylov, A. I.; Zimmerman, P. M.; Casanova, D. Calculation of Spin–orbit Couplings Using RASCI Spinless One-particle Density Matrices: Theory and Applications. *J. Chem. Phys.* **2020**, *153*, 214107.

(52) Malmqvist, P. Å.; Roos, B. O.; Schimmelpfennig, B. The Restricted Active Space (RAS) State Interaction Approach with Spin-orbit Coupling. *Chem. Phys. Lett.* **2002**, *357*, 230–240.

(53) Malmqvist, P. Å.; Roos, B. O. The CASSCF State Interaction Method. *Chem. Phys. Lett.* **1989**, *155*, 189–194.

(54) Valentine, A. J. S.; Li, X. Toward the Evaluation of Intersystem Crossing Rates with Variational Relativistic Methods. *J. Chem. Phys.* **2019**, *151*, 084107.

(55) Dyall, K. G.; Fægri, Jr., K. *Introduction to Relativistic Quantum Chemistry*; Oxford University Press, 2007.

(56) Tamukong, P. K.; Hoffmann, M. R.; Li, Z.; Liu, W. Relativistic GVVPT2 Multireference Perturbation Theory Description of the Electronic States of $Y_2$ and $Tc_2$. *J. Phys. Chem. A* **2014**, *118*, 1489–1501.

(57) Boettger, J. C. Approximate Two-Electron Spin-Orbit Coupling Term For Density-Functional-Theory DFT Calculations Using The Douglas-Kroll-Hess Transformation. *Phys. Rev. B* **2000**, *62*, 7809–7815.

(58) Pierloot, K. The CASPT2 Method in Inorganic Electronic Spectroscopy: from Ionic Transition Metal to Covalent Actinide Complexes. *Mol. Phys.* **2003**, *101*, 2083–2094.

(59) Roos, B. O.; Lindh, R.; Malmqvist, P.-Å.; Veryazov, V.; Widmark, P.-O. *Multiconfigurational Quantum Chemistry*; Wiley, 2016.

(60) Frisch, M. J.; Trucks, G. W.; Schlegel, H. B.; Scuseria, G. E.; Robb, M. A.; Cheeseman, J. R.; Scalmani, G.; Barone, V.; Petersson, G. A.; Nakatsuji, H.; Li, X.; Caricato, M.; Marenich, A. V.; Bloino, J.; Janesko, B. G.; Gomperts, R.; Mennucci, B.; Hratchian, H. P.; Ortiz, J. V.; Izmaylov, A. F.; Sonnenberg, J. L.; Williams-Young, D.; Ding, F.; Lipparini, F.; Egidi, F.; Goings, J.; Peng, B.; Petrone, A.; Henderson, T.; Ranasinghe, D.; Zakrzewski, V. G.; Gao, J.; Rega, N.; Zheng, G.; Liang, W.; Hada, M.; Ehara, M.; Toyota, K.; Fukuda, R.; Hasegawa, J.; Ishida, M.; Nakajima, T.; Honda, Y.; Kitao, O.; Nakai, H.; Vreven, T.; Throssell, K.; Montgomery, J. A., Jr.;

Peralta, J. E.; Ogliaro, F.; Bearpark, M. J.; Heyd, J. J.; Brothers, E. N.; Kudin, K. N.; Staroverov, V. N.; Keith, T. A.; Kobayashi, R.; Normand, J.; Raghavachari, K.; Rendell, A. P.; Burant, J. C.; Iyengar, S. S.; Tomasi, J.; Cossi, M.; Millam, J. M.; Klene, M.; Adamo, C.; Cammi, R.; Ochterski, J. W.; Martin, R. L.; Morokuma, K.; Farkas, O.; Foresman, J. B.; Fox, D. J. Gaussian Development Version Revision I.11+.

(61) Noro, T.; Sekiya, M.; Koga, T. Segmented Contracted Basis Sets for Atoms H Through Xe: Sapporo-(DK)-nZP Sets (n = D, T, Q). *Theor. Chem. Acc.* **2012**, *131*, 1124.

(62) Pinjari, R. V.; Delcey, M. G.; Guo, M.; Odelius, M.; Lundberg, M. Erratum: "Restricted Active Space Calculations of L-edge X-ray Absorption Spectra: From Molecular Orbitals to Multiplet States" [J. Chem. Phys. 141, 124116 (2014)]. *J. Chem. Phys.* **2015**, *142*, 069901.

(63) Wang, H.; Bokarev, S. I.; Aziz, S. G.; Kühn, O. Ultrafast Spin-State Dynamics in Transition-Metal Complexes Triggered by Soft-X-Ray Light. *Phys. Rev. Lett.* **2017**, *118*, 023001.

(64) Atak, K.; Bokarev, S. I.; Gotz, M.; Golnak, R.; Lange, K. M.; Engel, N.; Dantz, M.; Suljoti, E.; Kühn, O.; Aziz, E. F. Nature of the Chemical Bond of Aqueous $Fe^{2+}$ Probed by Soft X-ray Spectroscopies and Ab Initio Calculations. *J. Phys. Chem. B* **2013**, *117*, 12613–12618.

(65) Grell, G.; Bokarev, S. I.; Winter, B.; Seidel, R.; Aziz, E. F.; Aziz, S. G.; Kühn, O. Multireference Approach to the Calculation of Photoelectron Spectra Including Spin-orbit Coupling. *J. Chem. Phys.* **2015**, *143*, 074104.

(66) Golnak, R.; Bokarev, S. I.; Seidel, R.; Xiao, J.; Grell, G.; Atak, K.; Unger, I.; Thürmer, S.; Aziz, S. G.; Kühn, O.; Winter, B.; Aziz, E. F. Joint Analysis of Radiative and Non-radiative Electronic Relaxation upon X-ray Irradiation of Transition Metal Aqueous Solutions. *Sci. Rep.* **2016**, *6*, 24659.

(67) Fouqueau, A.; Mer, S.; Casida, M. E.; Lawson Daku, L. M.; Hauser, A.; Mineva, T.; Neese, F. Comparison of Density Functionals for Energy and Structural Differences Between the High-[$^5T_{2g}$:$(t_{2g})^4(e_g)^2$] and Low-[$^1A_{1g}$:$(t_{2g})^6(e_g)^0$] Spin States of the Hexaquoferrous Cation $[Fe(H_2O)^6]^{2+}$. *J. Chem. Phys.* **2004**, *120*, 9473–9486.

(68) Fouqueau, A.; Casida, M. E.; Daku, L. M. L.; Hauser, A.; Neese, F. Comparison of Density Functionals for Energy and Structural Differences Between the High-[$^5T_{2g}$:$(t_{2g})^4(e_g)^2$] and Low-[$^1A_{1g}$:$(t_{2g})^6(e_g)^0$] Spin States of Iron(II) Coordination Compounds. II. More Functionals and the Hexaminoferrous Cation, $[Fe(NH_3)^6]^{2+}$. *J. Chem. Phys.* **2005**, *122*, 044110.

(69) Miedema, P. S.; de Groot, F. M. The iron L edges: Fe 2p X-ray absorption and electron energy loss spectroscopy. *J Electron Spectros Relat Phenomena* **2013**, *187*, 32–48.

(70) de Groot, F. Multiplet effects in X-ray Spectroscopy. *Coord. Chem. Rev.* **2005**, *249*, 31–63.

(71) Pollak, P.; Weigend, F. Segmented Contracted Error-Consistent Basis Sets of Double- and Triple-Valence Quality for One- and Two-Component Relativistic All-Electron Calculations. *J. Chem. Theory Comput.* **2017**, *13*, 3696–3705.

(72) Kristine, P.; Eftimios, T.; Björn O., R. 3P-3D Intershell Correlation Effects in Transition Metal Ions. *Chem. Phys. Lett.* **1993**, *214*, 583–590.

(73) Kowalska, J. K.; Nayyar, B.; Rees, J. A.; Schiewer, C. E.; Lee, S. C.; Kovacs, J. A.; Meyer, F.; Weyhermüller, T.; Otero, E.; DeBeer, S. Iron L2,3-Edge X-ray Absorption and X-ray Magnetic Circular Dichroism Studies of Molecular Iron Complexes with Relevance to the FeMoco and FeVco Active Sites of Nitrogenase. *Inorg. Chem.* **2017**, *56*, 8147–8158.

(74) Per-Olof, W.; B. Joakim, P.; Björn O., R. Density Matrix Averaged Atomic Natural

Orbital (ANO) Basis Sets for Correlated Molecular Wave Functions II. Second Row Atoms. *Theor. Chem. Acc.* **1991**, *79*, 419–432.

(75) Rosendo, P.-A.; Manuela, M.; Ignacio, N.-G.; Per-Olof, W.; Björn O., R. Density Matrix Averaged Atomic Natural Orbital (ANO) Basis Sets for Correlated Molecular Wave Functions III. First Row Transition Metal Atoms. *Theor. Chem. Acc.* **1995**, *92*, 149–181.

(76) Wasinger, E. C.; de Groot, F. M.; Hedman, B.; Hodgson, K. O.; Solomon, E. I. L-edge X-ray Absorption Spectroscopy of Non-heme Iron Sites: Experimental Determination of Differential Orbital Covalency. *J. Am. Chem. Soc.* **2003**, *125*, 12894–12906.
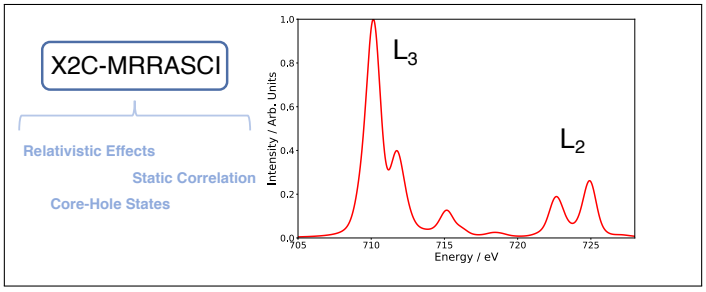
# Graphical TOC Entry